

**Theoretical investigation of measuring cerebral blood
flow in the adult human head using bolus indocyanine
green injection and near-infrared spectroscopy**

Terence S. Leung, Ilias Tachtsidis, Martin Tisdall,*

Martin Smith*, David T. Delpy, Clare E. Elwell

Department of Medical Physics & Bioengineering, University College London, Gower
Street, London WC1E 6BT, U.K.

*Department of Neuroanaesthesia & Neurocritical Care, The National Hospital for
Neurology & Neurosurgery, London, U.K.

Abstract

To investigate the accuracy of measuring cerebral blood flow (CBF) using a bolus injection of indocyanine green (ICG) detected by near infrared spectroscopy in adult human heads, simulations were performed using a two layered model, representing the extracerebral and intracerebral layers. Modelled optical data were converted into tissue ICG concentration using either the one detector modified Beer Lambert law (MBLL) method, or the two detector partial pathlength (PPL) method. CBFs were estimated using deconvolution and blood flow index techniques respectively. Using the MBLL method, CBFs were significantly underestimated but the PPL method improved their accuracy and robustness, especially when used as relative measures. Dispersion of the arterial input function also affected the CBF estimates.

OCIS codes: 170.3660, 170.3890, 170.6510

1. Introduction

The measurement of cerebral blood flow (CBF) is a crucial tool in assessing cerebral well being especially in pathological patients. Regional CBF can be measured with imaging techniques such as dynamic susceptibility contrast magnetic resonance imaging (MRI), Xenon CT and positron emission tomography (PET). These techniques provide a map of CBF for the whole brain but are of limited use to critically ill patients in the intensive care unit who cannot be easily transferred to such scanners. High operating costs also restrict their availability and for the latter two methods radiation exposure limits the number of studies that can be made. For these reasons, measuring CBF optically at the bedside using near infrared spectroscopy (NIRS) is an attractive alternative. The NIRS technique involves placing one or more optical sources and detectors on the surface of the head overlying the cerebral region of interest. Although only producing a single point measurement instead of a 2D cross sectional map as provided by other imaging modalities, this technique in principle provides a relatively fast, simple and inexpensive way to measure localised CBF.

While the NIRS measurement of a relative CBF (arbitrary units) can be performed using diffusion correlation spectroscopy,¹ an absolute CBF (units of ml/100g/min) has to be measured using tracer tracking techniques. Two main tracers have been used in NIRS, namely, oxy-haemoglobin² and indocyanine green (ICG).^{3,4} The use of oxy-haemoglobin as a tracer involves first slightly lowering the subject's inspired oxygen fraction, and then sharply increasing it to produce a bolus of oxy-haemoglobin flowing into the brain which acts as the tracer. For the first few seconds, the venous outflow of the tracer can be

assumed to be zero and the CBF can be calculated from the measurement of changes in arterial oxygen saturation and tissue oxy-haemoglobin concentrations using the Fick principle. The need to reduce oxygen intake can make this technique unsuitable for patients with brain injury, in whom CBF is most likely to be measured. Also since only a few seconds worth of data are used for the CBF calculation, the technique has a large coefficient of variation.^{2,5}

Another tracer often used is ICG which is a contrast agent with high absorption in the near-infrared range and this produces a signal with a greater signal-to-noise ratio than oxy-haemoglobin. To perform a CBF measurement, a bolus of ICG is injected intravenously, and the arterial ICG concentration may be recorded by a non-invasive pulse-dye densitometer with the probe attached to a peripheral site (e.g. ear lobe, finger or nose), or by an invasive intra-arterial probe. The tissue ICG concentration is measured by a NIRS spectrometer with the probe placed on the head overlying the region of interest. There are four main approaches to the calculation of CBF from the recorded arterial and tissue ICG concentrations. The first approach makes use of only the first few seconds of data when the venous outflow of ICG can be assumed to be zero,⁴ and is similar to the method used when oxy-haemoglobin is used as the tracer. The CBF can then be calculated by applying the Fick principle. This approach suffers from the same robustness problem as the oxy-haemoglobin tracer technique because of the relatively short amount of data considered in the calculation.

The second approach considers the slope of the initial rise of the tissue ICG concentration curve, termed the blood flow index (BFI),⁶⁻⁹ as an index of CBF. However, BFIs are only comparable when the optical properties of the measurement sites, the geometry and the circulating blood volume are the same. This is only true during repeated measurements within the same subject. This means that BFIs can only be used as a trend measure to compare CBFs at different times in the same subject with a stable cerebral blood volume but not as an absolute measure of CBFs among different subjects. Another limitation is that for a valid comparison between different BFI measurements, their arterial input functions (AIFs) have to be exactly the same which can be difficult to achieve in practice. Zierler¹⁰ discussed the changes in tissue concentration of a tracer as a function of time and pointed out that the tissue time-concentration curve reflects not only the vascular physiology of the tissue but also the AIF. The BFI is calculated from the initial up slope of the tissue time-concentration curve and does not consider the input arterial function (the arterial ICG bolus) at all. Using BFIs with different AIFs to compare CBFs will therefore introduce significant errors.

The third approach exploits the concept of the impulse residue function (IRF) which carries information about the mean transit time (MTT), CBF and volume. The IRF is the tracer concentration deposited in tissue when a unit bolus of tracer is injected instantaneously in the arterial site, resembling a delta function.¹¹ To recover the IRF, the arterial and tissue ICG concentrations are measured and used for deconvolution. Brown *et al*¹² performed deconvolution with the constraints that the deconvolved IRF was non negative and has a flat plateau followed by a decreasing function. The study compared

the CBF estimated by using NIRS ICG measurements and using CT measurements in six newborn piglets. Paired t-tests showed no significant difference.

The fourth approach was reported by Keller *et al*¹³ who derived the venous outflow as the convolution of the arterial inflow and the transport function modelled as a logarithmic normal density function. Using the Fick principle, it was claimed that both the arterial inflow and venous outflow can be estimated from the measured tissue ICG concentration, and accordingly the *MTT* can also be found. The cerebral blood volume was calculated as the division of the tissue ICG concentration by the arterial ICG concentration. Finally, CBF was derived by dividing the CBV by the *MTT*. This study also compared the absolute CBFs measured by NIRS and perfusion weighted MRI in 6 subjects and found some agreement (the differences against their mean are within two standard deviations).

The NIRS technique may seem attractive but it poses several challenges when applied to the adult human head. First, its non-invasive nature means that a measurement is taken from the surface of the head and the measurement is subsequently contaminated by an unknown amount of extracerebral blood flow. Second, the AIF is normally measured at a peripheral site and is assumed to mimic the AIF feeding the arteries entering the field of view where the CBF is measured, i.e. the carotid or middle cerebral arteries. As a result, any dispersion of the AIF between the two sites will affect the CBF estimate. These issues have particular implications for CBF measurements in adults who have thick scalp and skull, and a more substantial external vasculature.

A study using ICG and NIRS found a mean CBF of 8.3 ml/100g/min in 12 healthy adult volunteers using the IRF (deconvolution) method.⁷ This value is very low compared to the CBF value of around 60 ml/100g/min as reported by other measurement techniques such as MRI bolus tracking and Xenon CT. Indeed, some studies have concluded that measuring CBF with NIRS techniques is unreliable.^{5,14}

Most of the published papers on measuring CBF with NIRS and ICG are experimental studies based on one of the techniques described earlier. To address the two issues raised above, it is necessary to conduct experiments under strictly controlled conditions with known variables and this is very difficult to carry out in practice. We have therefore used physiologically and experimentally informed computer simulations, which are based on an analytical model of light transport in a two layered medium proposed by Kienle *et al.*¹⁵ Both optical attenuation and mean time delay (expressed as a phase delay for a modulated source signal) were calculated.

2. Methods

A. *The physiological model*

1. *The indicator-dilution theory*

The indicator-dilution theory considers a tracer being injected into the blood stream and mathematically relates the blood flow F , the AIF $C_{art}(t)$ and the tissue time-concentration curve, $C_{tis}(t)$ using the concept of the IRF, $R(t)$:¹⁶

$$C_{tis}(t) = F \int_0^t C_{art}(\tau) R(t - \tau) d\tau \quad (1)$$

where t is time and τ is an integration variable. The IRF corresponds to the amount of tracer deposited in the tissue, i.e. $C_{tis}(t)$ when the AIF is a Dirac delta function (its integral equals to one at the time of input and zero at all other times). The first moment of $R(t)$ is the MTT and the blood volume (V) is $V = MTT \times F$ according to the central volume principle.¹⁶ In the context of this study, the AIF corresponds to $[ICG(t)]_{art}$ and the tissue time-concentration curves correspond to $[ICG(t)]_{ext}$ and $[ICG(t)]_{int}$ for the extracerebral layer and the intracerebral layer respectively. Based on this formulation, we can incorporate known values of blood flow and MTT together with a modelled $[ICG(t)]_{art}$, which we simulated based on experimental data, to generate $[ICG(t)]_{ext}$ and $[ICG(t)]_{int}$.

2. *Physiological parameters*

Table 1 lists the values of blood flow, blood volume and MTT used in the simulations. Other parameters in the table will be further discussed in section 2.B.2. Using the XeCT technique, the blood flow in the extracerebral layer was reported to be 5-8 ml/100g/min.¹⁷

A mean value of 6.5 ml/100g/min has been used here. In another study, the mean absolute oxy and deoxy-haemoglobin concentration in the forehead were found to be 6.4 and 4.3 μM respectively using near infrared spatially resolved spectroscopy with an optical probe having one source and nine detectors (SD spacings ranging from 1.75 to 16.79 mm).¹⁸ The total absolute tissue haemoglobin concentration (i.e. 10.7 μM) was converted to the blood volume of 0.7 ml/100g for the extracerebral layer in Table 1. The conversion involves the use of a nominal blood haemoglobin concentration of 14 g/dl and a small-to-large-vessel-haematocrit-ratio of 0.69.¹⁹ The values for the blood flow and volume in the brain were obtained from a MRI CBF simulation study by Calamante *et al*²⁰ who found them suitable for simulating the blood flow and volume in the grey matter.

3. *Simulation of the arterial input function*

The experimental $[\text{ICG}(t)]_{\text{art}}$ was measured by a pulse dye-densitometer (DDG-2001, Nihon Kohden) with a nasal probe on a healthy adult volunteer. We found by visual inspection that the log normal function, which has been used to approximate the arterial input function in the estimation of cardiac output,²¹ also sufficiently fits the first pass of our experimentally measured $[\text{ICG}(t)]_{\text{art}}$. One empirical feature we found in the time-concentration curve of the NIRS measured signal is that the recirculation is more dominant than that measured by other techniques such as MRI and CT. We therefore also consider the recirculation and $[\text{ICG}(t)]_{\text{art}}$ is modelled as the summation of three log normal functions.

$$\begin{aligned}
[ICG(t)]_{art} &= \sum_{n=1}^3 A_n \exp[-k_n f(t, t_n)^2] \\
f(t, t_n) &= \begin{cases} \ln[(t - \tau_n)/t_n] & \text{for } t \geq \tau_n \\ 0 & \text{otherwise} \end{cases}
\end{aligned} \tag{2}$$

where $A_1=11.5$, $k_1=2.6$, $t_1=4.2$, $\tau_1=0$, $A_2=1.1$, $k_2=0.25$, $t_2=25$ s, $\tau_2=15$ s, $A_3=0.8$, $k_3=4$, $t_3=25$ s and $\tau_3=1$ s. The modelled and experimentally measured $[ICG(t)]_{art}$ are plotted in Figure 1(a) for comparison. Another widely used model for the arterial input function is the gamma variate function.^{20,22}

4. Simulation of the impulse residue functions

A simple and widely used model for the IRF in tissue is the exponential function which considers the vasculature bed as one single and well-mixed compartment. It has been used to model the IRF in the brain.^{20,22} $R(t) = \exp(-t / MTT)$ where $t \geq 0$ and the first moment of $R(t)$ is MTT . From the measurement site to the site where ICG enters the arteries feeding the tissue in the field of view, $[ICG(t)]_{art}$ may be dispersed. The dispersion can be modelled by convolving $R(t)$ with a dispersion function $\exp(-t/\beta)/\beta$ and the effective IRF becomes.²⁰

$$R(t) = \frac{MTT}{(\beta - MTT)} [\exp(-t / \beta) - \exp(-t / MTT)] \tag{3}$$

where $t \geq 0$ and β is the dispersion factor with the units of seconds.

5. *Simulation of the tissue ICG concentration curves*

Using the AIF model, the IRFs, and the *MTT* and blood flow values shown in Table 1, $[ICG(t)]_{ext}$ and $[ICG(t)]_{int}$ can be simulated as shown in Figure 1(b). It can be seen that $[ICG(t)]_{ext}$ is more dispersed and has a lower peak value which agrees with the general behaviour of the tissue tracer time-concentration curve in the extracerebral layer found in a MRI study.²³

B. *The optical model*

1. *Two layered analytical model*

To simulate the light propagation in the extracerebral layer and the intracerebral layer, a 2 layered model for frequency domain measurements proposed by Kienle *et al*¹⁵ has been adopted. Given the depth of the first layer, the modulation frequency (f_{mod}), the absorption coefficients (μ_a) and reduced scattering coefficients (μ_s') in the upper and lower layers, this model can predict the reflectance (r) at a pre-defined SD spacing and the phase angle (θ) between the source and detector. The model assumes a flat geometry both at the surface and at the boundary between the upper and lower layers, and that the lower layer is infinitely thick. It also assumes a tissue-air refractive index mismatch.

2. Optical parameters

Using the 2 layered model, we can predict both the reflectance and phase angles at different surface measurement points with assigned μ_a and μ_s' in the two layers. In this section, the two optical coefficients are expressed as $\mu_a(\lambda)$ and $\mu_s'(\lambda)$ to highlight their wavelength dependency. Two equations have been used to form $\mu_a(\lambda)$ in each layer. The first equation calculates the $\mu_a(\lambda)$ before the ICG enters the field of view and is denoted by $\mu_a^0(\lambda)$ here:

$$\mu_a^0(\lambda) = \varepsilon_{HHb}(\lambda)[HbT](1 - SO_2) + \varepsilon_{HbO_2}(\lambda)[HbT] \cdot SO_2 + \mu_{a,H_2O}(\lambda)W + \mu_a^{bk} \quad (4)$$

where $\varepsilon_{HHb}(\lambda)$ and $\varepsilon_{HbO_2}(\lambda)$ are the specific absorption coefficients of deoxy- and oxy-haemoglobin ($\mu\text{M}^{-1} \text{mm}^{-1}$), $[HbT]$ is the total haemoglobin concentration (μM), SO_2 is the tissue oxygenation (as a fraction), W is the water content (as a fraction), and $\mu_{a,H_2O}(\lambda)$ is the absorption coefficient of 100% water (mm^{-1}), and μ_a^{bk} is a wavelength independent background absorption (mm^{-1}). It is assumed that the physiology does not change over time and subsequently these parameters are assumed to be time invariant. The values of $[HbT]$ and W for each layer are listed in Table 1. The water content of each layer has been measured previously using the MRI technique.²⁴ The SO_2 for the two layers have been set to a nominal value of 0.7. The $\mu_a(\lambda)$ in the two layers calculated using these parameters were smaller than those used by Okada and Delpy.²⁵ A wavelength independent background μ_a^{bk} was therefore added so that the total value matched those in Okada and Delpy²⁵ at 800 nm, i.e. the μ_a^{bk} for the extracerebral layer = 0.015 mm^{-1} and the μ_a^{bk} for

the intracerebral layer = 0.023 mm⁻¹. The existence of the background absorption has been previously discussed by Essenpreis *et al*²⁶ and Hueber *et al*.²⁷ Using these values, the total extracerebral $\mu_a(800nm) = 0.018 \text{ mm}^{-1}$ and the total intracerebral $\mu_a(800nm) = 0.036 \text{ mm}^{-1}$ which were the same values used in Okada and Delpy.²⁵ For comparison, this approach also resulted in extracerebral and intracerebral $\mu_a(759nm)$ of 0.019 mm⁻¹ and 0.037 mm⁻¹ respectively which are comparable to the experimentally found extracerebral and intracerebral $\mu_a(759nm)$ of 0.015 mm⁻¹ and 0.030 mm⁻¹ found in a previous study.²⁸

When ICG enters the field of view, a time variant absorption change is introduced and the corresponding μ_a , i.e. $\mu_a^{ICG}(t, \lambda)$ can be modelled as:

$$\mu_a^{ICG}(t, \lambda) = \mu_a^0(\lambda) + [ICG(t)]\varepsilon_{ICG}(\lambda) \quad (5)$$

where $\varepsilon_{ICG}(\lambda)$ is the specific absorption coefficient of ICG. The [ICG(t)] here corresponds to either [ICG(t)]_{ext} or [ICG(t)]_{int} whose generation has been discussed in section 2.A. The values of $\varepsilon_{HHb}(\lambda)$, $\varepsilon_{HbO_2}(\lambda)$, $\varepsilon_{ICG}(\lambda)$ and $\mu_{a,H_2O}(\lambda)$ used here were obtained from previous measurements performed in our laboratory^{4,29}. It should be noted that all the absorption coefficients here are based on the log base of e , rather than 10, in order to be consistent with the diffusion theory.

For the $\mu_s'(\lambda)$ in the extracerebral layer, we employed an expression derived by Doornbos *et al*¹⁸ who conducted spatially resolved spectroscopy measurement on the

human forehead: $\mu_s^{ext}(\lambda) = a(\lambda \times 10^{-3})^{-b} \times 10^{-3}$ where $a = 1141$, $b = 0.84$ and λ is in nm. In this study, the maximum SD spacing is 16.79 mm and the results are mainly applicable to the extracerebral layer.

van der Zee *et al*³⁰ measured μ_s' for brain tissues *in vitro* at 800 nm. Matcher *et al*³¹ measured $\mu_s'(\lambda)$ in the adult human forehead *in vivo* using time resolved spectroscopy with a SD spacing of 40 mm which was believed to probe both the extracerebral layer and the intracerebral layer. Here, we used $\mu_s'(800nm) = 2.2 \text{ mm}^{-1}$ for the grey matter found by van der Zee *et al*³⁰ as the reference value and adopted the wavelength dependency found by Matcher *et al*³¹ to calculate $\mu_s'(\lambda)$ at other wavelengths. The formulation of $\mu_s'(\lambda)$ in the intracerebral layer is written as: $\mu_s^{int}(\lambda) = 2.2(\lambda a + b)/(800a + b)$ where $a = -6.5 \times 10^{-4}$, $b = 1.45$ and λ in nm. For $\lambda = 800 \text{ nm}$, $\mu_s^{int}(\lambda) = 2.2 \text{ mm}^{-1}$.

Using the techniques discussed in this section, the reflectance and phase angles were predicted at 775, 813 and 853 nm which were three of the wavelengths used in the spectrometer during our previous *in vivo* study.⁷ The attenuations were calculated from reflectance, i.e. $A = -\log_e(r)$ and the total mean pathlength calculated from the phase angles, i.e. $L = \theta/(2\pi f_{mod} c_{tis})$ where c_{tis} is the speed of light in tissue. The optical data were predicted at 2 measurement points with SD spacings of 45 and 50 mm which were chosen to be the same as the configuration of the optodes used in our previous study.⁷

Before ICG entered the field of view, the pathlength at a SD spacing of 50 mm is 310 mm at 813 nm which corresponds approximately to a differential pathlength factor

(DPF) of 6.2. This value agrees reasonably well with the experimental finding of 6.1 at 807 nm, using the age dependent equation of $DPF = 4.99 + 0.067A^{0.814}$ where A (age) = 30 years,³² and adds to our confidence that the 2 layered analytical model and the optical and physiological parameters used (as shown in Table 1) are suitable.

C. Conversion of optical data to concentrations

1. The modified Beer Lambert law (MBLL) method

One widely used technique to convert attenuation into ICG concentration is by using the modified Beer Lambert law: $\Delta \mathbf{C} = \boldsymbol{\epsilon}^{-1} \Delta \mathbf{A} / L$ where L is the optical mean pathlength, $\Delta \mathbf{C}$ is a column vector containing the changes in concentrations of ICG, deoxy- (HHb) and oxy-haemoglobin (HbO_2), i.e. $[\Delta C_{ICG} \Delta C_{HHb} \Delta C_{HbO_2}]^T$, $\boldsymbol{\epsilon}^{-1}$ is the inverse of a matrix containing the specific absorption coefficients of ICG, HHb and HbO_2 at different wavelengths, and $\Delta \mathbf{A}$ is a column vector containing changes in attenuations at different wavelengths. In this work, $\Delta \mathbf{A} = [A^{ICG}(\lambda_1) - A^0(\lambda_1), A^{ICG}(\lambda_2) - A^0(\lambda_2), A^{ICG}(\lambda_3) - A^0(\lambda_3)]^T = [\Delta A(\lambda_1), \Delta A(\lambda_2), \Delta A(\lambda_3)]^T$ where $A^0(\lambda)$ and $A^{ICG}(\lambda)$ are attenuations before and after ICG enters the field of view, and the three wavelengths used are 775, 813 and 853 nm. Since the concentrations of HHb and HbO_2 are set to be constant before and after the appearance of ICG, it is expected the resulting ΔC_{HHb} and ΔC_{HbO_2} are close to zero. It should be noted that L is in fact wavelength dependent but a fixed value is often used and scaling factors correcting for the wavelength dependency are incorporated in $\boldsymbol{\epsilon}$. This formulation assumes a homogenous medium. In this paper, we refer the use of a single detector measurement and the modified Beer Lambert law as the MBLL method.

2. The partial pathlength (PPL) method

Hiraoka *et al*³³ introduced the concept of partial pathlengths to extend the modified Beer Lambert law to heterogeneous media. The partial pathlength of a layer is defined as a partial derivative of the measured A versus the μ_a at that layer and can be considered as the mean pathlength that light has travelled in that layer. For a two layered model with two detectors, we have

$$\begin{bmatrix} \Delta A_1(\lambda) \\ \Delta A_2(\lambda) \end{bmatrix} = \begin{bmatrix} \rho_{1,1}(\lambda) & \rho_{1,2}(\lambda) \\ \rho_{2,1}(\lambda) & \rho_{2,2}(\lambda) \end{bmatrix} \begin{bmatrix} \Delta \mu_{a,1}(\lambda) \\ \Delta \mu_{a,2}(\lambda) \end{bmatrix} \quad (6)$$

where $\Delta A_1(\lambda)$ and $\Delta A_2(\lambda)$ are the changes of attenuation (i.e. $A^{ICG}(\lambda) - A^0(\lambda)$) measured by detector 1 and 2, $\Delta \mu_{a,1}(\lambda)$ and $\Delta \mu_{a,2}(\lambda)$ are the changes of absorption coefficient in layer 1 (upper) and 2 (lower), $\rho_{m,n}(\lambda)$ is the partial pathlengths at layer n as measured by detector m ($m, n = 1$ or 2). Subsequently, $\Delta \mu_a(\lambda)$ in both layers can be estimated by: $\Delta \mathbf{M} = \mathbf{R}^{-1} \Delta \mathbf{A}$ where $\Delta \mathbf{M} = [\Delta \mu_{a,1}(\lambda), \Delta \mu_{a,2}(\lambda)]^T$ and \mathbf{R} is the matrix containing all the partial pathlengths $\rho_{m,n}(\lambda)$ in equation (6). The partial pathlengths, however, cannot be measured directly but can be estimated iteratively with Monte Carlo simulations or a solution of the diffusion equation using frequency or time domain measurements²⁸. In this work, they are estimated by $\rho_{1,1}(\lambda) = \Delta A_1(\lambda) / \Delta \mu_{a,1}(\lambda)$ where $\Delta \mu_{a,1}(\lambda)$ is set to a small value, e.g. 0.001 and $\Delta A_1(\lambda)$ is the corresponding change of attenuation predicted by the optical model, and subsequently, $\rho_{1,2}(\lambda) = L_1(\lambda) - \rho_{1,1}(\lambda)$. The corresponding physiological and optical

parameters are the baseline values as shown in Table 1. Both $\rho_{2,1}(\lambda)$ and $\rho_{2,2}(\lambda)$ can be found similarly. Once the $\Delta\mu_a(\lambda)$ in the brain, i.e. $\Delta\mu_{a,2}(\lambda)$ becomes available, the corresponding concentrations can be calculated by: $\Delta C = \epsilon^{-1} \Delta \mu_{a,2}$. In this paper, we refer to the use of two detector measurements and the partial pathlength formulation as the PPL method. As an example, using the modelling techniques described here and parameters in Table 1, the partial pathlength in the brain and the mean pathlength were estimated to be 18.8 and 254.5 mm for $\lambda=775$ nm, SD spacing = 45 mm and the thickness of the first layer = 8 mm. The ratio of partial to mean pathlength is 0.069. For comparison, a previous study²⁸, in which a time-resolved spectrometer and Monte Carlo simulations were used, found the partial pathlength in the brain and the mean pathlength of an adult subject to be 26.4 and 206.6 mm for $\lambda=759$ nm, SD spacing = 30 mm and the thickness of the scalp and skull = 7.9 mm. The corresponding ratio of partial to mean pathlength is 0.128. The discrepancies between these results can be attributed to different assumptions and optical properties used.

Using either the MBLL method or the PPL method, the tissue ICG concentration can be calculated. When the MBLL method is used, the notation $[ICG(t)]_{det2}$ is used to denote the tissue ICG concentration as measured by detector 2 (SD spacing = 50 mm). When the PPL method is used, the notation $[ICG(t)]_{det1\&2}$ is used to indicate both detectors 1 (SD spacing = 45 mm) and 2 are used. Figure 2 depicts $[ICG(t)]_{det2}$ and $[ICG(t)]_{det1\&2}$ predicted with three different dispersion factors in the intracerebral layer, (i.e. $\beta = 0, 0.5$ and 1 s) and an extracerebral thickness of 10 mm. It should be noted that $[ICG(t)]_{det2}$ accounts for a weighted average of the tissue ICG concentrations in the

extracerebral layer, i.e. $[ICG(t)]_{\text{ext}}$ and the intracerebral layer, $[ICG(t)]_{\text{int}}$ because of the assumption of a homogenous medium. On the other hand, $[ICG(t)]_{\text{det1\&2}}$ corresponds to $[ICG(t)]_{\text{int}}$ only, due to the 2 layer assumption. It will be shown in section 3 that the PPL method will provide CBF estimates less sensitive to the extracerebral blood flow. It can be seen from Figure 2(a) that $[ICG(t)]_{\text{det2}}$ is more dispersed and has a lower peak value, bearing more similarities to $[ICG(t)]_{\text{ext}}$ than $[ICG(t)]_{\text{int}}$ (c.f. Figure 1(a)). This indicates the influence of the extracerebral blood flow on $[ICG(t)]_{\text{det2}}$. On the other hand, $[ICG(t)]_{\text{det1\&2}}$ in Figure 2(b) is more similar qualitatively to $[ICG(t)]_{\text{int}}$ showing a high sensitivity to intracerebral changes.

D. Estimation of cerebral blood flow

1. Deconvolution

Re-writing equation (1) in discrete form for the tracer ICG,

$$[ICG(t_j)]_{\text{tis}} = \Delta t \cdot F \cdot \sum_{i=0}^j [ICG(t_i)]_{\text{art}} \cdot R(t_j - t_i) \quad (7)$$

where $[ICG(t)]_{\text{tis}}$ is the tissue ICG concentration measured by either the MBLL method or the PPL method as discussed in the last section, and Δt is the sampling interval. Deconvolution is basically a numerical process to recover $F \cdot R(t)$ from measurements $[ICG(t)]_{\text{art}}$ and $[ICG(t)]_{\text{tis}}$. The singular value decomposition (SVD) approach has been used to perform deconvolution in general³⁴ and in CBF measurements with MRI bolus

tracking.³⁵ The SVD has a threshold which allows it to handle noisy data (a higher threshold for a higher level of noise) and maintain a stable solution. Since $R(t)$ has a maximum value of 1, the maximum value of $\mathbf{x} = [F \cdot R(t_0), F \cdot R(t_1), \dots, F \cdot R(t_{N-1})]^T$ is F , i.e. CBF. In actual measurements, there is a time delay between $[\text{ICG}(t)]_{\text{art}}$ measured at a peripheral site and $[\text{ICG}(t)]_{\text{tis}}$ measured over the head, potentially leading to erroneous results after deconvolution. The time delay can however be compensated for by manually synchronising the rise of the two curves.

2. *Blood flow index (BFI)*

As an alternative to deconvolution, relative CBF can be quantified using the BFI⁶ which is defined here as the gradient of $[\text{ICG}(t)]_{\text{tis}}$ during the initial inflow of ICG, i.e. the difference between the 90% and 10% of the peak value over the corresponding time interval.⁷

E. Numerical experiments

Three numerical experiments were performed to investigate different aspects of the CBF and BFI estimations:

Numerical experiment 1: The extracerebral blood flow was fixed at 6.5 ml/100g/min while the CBF was varied between -20% and +20% (steps of 10%) around the baseline value of 60 ml/100g/min.

Numerical experiment 2: The extracerebral blood flow was varied between -20% and +20% (steps of 10%) around the baseline value of 6.5 ml/100g/min while the CBF was fixed at 60 ml/100g/min.

Numerical experiment 3: Both the extracerebral blood flow and CBF were fixed at 6.5 and 60 ml/100g/min while the dispersion factor in the vasculature was varied between 0 and 1 s (steps of 0.5 s).

The dispersion factor in the vasculature was set to zero for numerical experiments 1 and 2. Table 2 summarises the values of all the parameters used in the three experiments. The values of other parameters such as the water content, background absorption and reduced scattering coefficients, were the same as those shown in Table 1. Kohl-Bareis *et al*²³ found that the MRI perfusion signals using gadolinium-DTPA as a tracer were more dispersed in shape at the extracerebral site than those at the intracerebral site. To incorporate this finding, a larger dispersion factor of 6 s was used for $R(t)$ in the extracerebral layer. Also, $R(t)$ was normalised to give a maximum value of one so that the maximum value of the deconvolved $F \cdot R(t)$ corresponds to the extracerebral blood flow. In each numerical experiment, the optical data (attenuation and phase angle) were predicted from the two layered analytical model while the thickness of the upper layer was varied between 8 and 12 mm in steps of 2 mm.

In each numerical experiment, the predicted optical data were analysed by the MBLL method and the PPL method. When using the MBLL, the mean pathlength needs

to be calculated from the phase angle. Strictly speaking, the mean pathlength $L(t,\lambda)$ is both time and wavelength dependent. In reality, the experimentally measured phase angles are often very noisy which in turns affects the accuracy of the estimated $L(t,\lambda)$. Therefore, one average phase angle is often used for a period of time. In this work, we also used one phase angle (the point before ICG appears) at each wavelength generated by the 2 layered analytical model to calculate one $L(\lambda)$ for the entire tissue ICG time-concentration curve. To use the PPL method, the partial pathlengths in the upper and lower layers as measured by the two detectors, i.e. $\rho_{m,n}$ ($m, n=1$ or 2) were estimated using a first order approximation as described in section 2.C.2. The partial pathlengths are also time and wavelength dependent, i.e. $\rho_{m,n}(t,\lambda)$ but to estimate them accurately using experimental measurements we need to know the evolution of $\mu_a(t,\lambda)$ in the two layers which is in fact what we are trying to measure. Therefore, it was assumed that the partial pathlengths did not change significantly during the inflow and clearance of ICG, and they were estimated before the ICG appeared in the field of view. This assumption inevitably introduced certain errors which we will further discuss later. For both methods, the threshold in the deconvolution was set to a rather small value of 1% of the maximum singular value because no noise was present in the predicted data.

3. Results

This section reports the results obtained from the three numerical experiments. For each experiment, the estimated CBFs are given in both absolute unit (ml/100g/min) and relative unit (% change). The estimated absolute CBFs are biased to different degrees due to the presence of the extracerebral blood flow in all cases. However, the estimated

relative percentage changes in CBFs are in some cases quite accurate. For numerical experiments 1 and 2 (Figures 3 and 4), all the relative percentage changes were calculated with respect to the middle value (out of 5 values), while in experiment 3 (Figure 5) the results corresponding to the dispersion factor = 0 second (the first value) were used as the reference values.

The absolute BFI values in terms of $\mu\text{M/s}$ depend on the optical properties of the measurement site and the total circulating blood volume which are likely to be different in different subjects. Therefore, absolute BFIs cannot be compared between different subjects. Using BFI in the same subject at different times, relative percentage changes in BFIs are sufficient. We therefore only present results of relative percentage change in BFIs here but not the absolute values.

Figures 3, 4 and 5 show the results of the three numerical experiments. In all figures, the three panels on the left are results obtained using the MBLL method (single detector with 50 mm SD spacing) while the other three on the right obtained using the PPL method (two detectors with spacings of 45 and 50 mm respectively). An identity line (dotted line) was drawn, where appropriate, on each figure corresponding to the ideal CBF or BFI estimates.

A. Influence of the extracerebral blood flow on CBF and BFI estimation

In the first two numerical experiments, we investigated the influence of the extracerebral blood flow on the CBF and BFI estimation. Figure 3 shows the results of experiment 1 whereby the extracerebral blood flow was kept constant at 6.5 ml/100g/min and the real CBF was varied between -20% and 20% of its baseline value of 60 ml/100g/min. Using the MBLL, it can be seen from Figure 3(a) that all the estimated absolute CBFs are between 6.5 and 8.5 ml/100g/min which are close to the constant extracerebral blood flow at 6.5 ml/100g/min showing its influence on the CBF estimates. The relative percentage changes in the estimated CBFs and BFIs as shown in Figure 3(c) and (e) do show some small changes as the underlying real CBF varies (e.g. for extracerebral thickness at 8 mm, Figure 3(c) shows that the percentage change of estimated CBF is only $\pm 5\%$ for real CBF changes of $\pm 20\%$). However, the sensitivities are therefore small. This means that the percentage changes of both CBF and BFI are largely underestimated. The sensitivity of those results corresponding to a thinner extracerebral layer (e.g. 8 mm) is marginally higher. These results once again show that both CBF estimates and BFIs are dominated by the extracerebral blood flow which was kept constant in this experiment.

Using the PPL method, the estimated absolute CBFs are comparatively closer to the identity line as shown in Figure 3(b). As discussed in section 2.5, only the partial pathlengths before the appearance of ICG were estimated and used for the whole tissue ICG time-concentration curve. Although this approach makes this method more readily applicable in practice, the errors introduced resulted in the discrepancies between the absolute CBF estimates and the identity line. It is also the case that the thicknesses of the extracerebral layer has an effect on these absolute CBF estimates and in this example the

absolute CBF estimates approach the identity line as the extracerebral layer thickness becomes larger, e.g. 12 mm. Figure 3(d) shows the relative percentage changes of CBFs and in all cases the estimates follow the identity line. Although not as good as its CBF counterpart, the percentage changes in BFIs still follow the identity line reasonably closely as shown in Figure 3(f). It is also noted that similar relative percentage changes are observed when different extracerebral layer thicknesses are used.

In numerical experiment 2, the CBF was kept constant at 60 ml/100g/min while the extracerebral blood flow was varied between -20% and +20% of its baseline value of 6.5 ml/100g/min. Using the MBL method, Figure 4(a) shows that the estimated absolute CBFs vary linearly between 5 and 9 ml/100g/min in all cases which again indicates the large influence of the extracerebral blood flow. Figure 4(c) further confirms the dominance of the varying extracerebral blood flows on the estimates and shows that the relative percentage changes of the CBF estimates closely follow the changes in the extracerebral blood flow. Figure 4(e) shows that the percentage changes in BFIs are equally affected by the varying extracerebral blood flows although in a non-linear fashion.

Figure 4(b) shows the absolute CBF estimates using the PPL method. It can be seen that the estimates are in general insensitive to changes in the extracerebral blood flow. The discrepancies between the real CBF at 60 ml/100g/min and the estimated values depend on the thickness of the extracerebral layer. In this example, the discrepancy is smallest when the thickness is 12 mm. The insensitivities of the CBF

estimates and the BFI to varying extracerebral blood flows are further illustrated in Figure 4(d) and (f) where the relative percentage changes are almost zero in all cases. It is also noted that similar relative percentage changes are observed when different extracerebral layer thicknesses are used.

B. Influence of the vasculature dispersion on CBF and BFI estimation

In numerical experiment 3, both the extracerebral blood flow and CBF were kept constant at 6.5 and 60 ml/100g/min respectively while the dispersion factor for the intracerebral layer was varied between 0 and 1 s (step size of 0.25 s). Figure 5(a), (c) and (e) show the results obtained using the MBLL method. As discussed earlier, the $[ICG(t)]_{tis}$ obtained using this method is dominated by the extracerebral blood flow and this is confirmed by Figure 5(a) in which the absolute CBF estimates are much smaller than the real CBF. Ideally, one would hope that the CBF estimates and BFIs would remain constant and not be altered by the dispersion, i.e. zero relative percentage changes. The relative percentage changes of CBF estimates and BFIs shown in Figure 5(c) and (e) increase by approximately 5 and 10 % respectively (for extracerebral thickness of 8 mm) as the dispersion factor increases from 0 to 1 s. These erroneous changes are in fact smaller than those obtained by the PPL method as shown in Figure 5(d) and (f). However, it does not mean that the MBLL method is more robust in the presence of dispersion but that $[ICG(t)]_{tis}$ calculated using the MBLL method is less sensitive to the intracerebral changes. This can be better explained by referring to Figure 2(a) in which $[ICG(t)]_{det2}$

($[ICG(t)]_{tis}$ measured by detector 2) corresponding to three dispersion factors in the intracerebral layer are plotted. It can be seen that their shapes are very similar to each other, indicating that any changes in the intracerebral layer has small influence on $[ICG(t)]_{det2}$.

Using the PPL method, the absolute CBF estimates reduce by a considerable amount as the dispersion factor increases from 0 to 1 s as shown in Figure 5(b). Figure 5(d) shows the relative percentage changes which are as much as -40% when the dispersion factor is 1 second. The strong effect of dispersion on the CBF estimates can be better appreciated by referring to Figure 2(b) which shows that $[ICG(t)]_{det1\&2}$ becomes more dispersed and has a lower peak value as the dispersion factor is increased from 0 to 1. These characteristics of the curves translate to a large reduction of CBF estimates after deconvolution. As for the BFI in Figure 5(f), the relative percentage changes are reduced by approximately -25% when the dispersion factor increases from 0 to 1 s. Since BFI is calculated from the initial rise of $[ICG(t)]_{det1\&2}$ and is not influenced by the dispersion of the remaining part of the curve, it turns out that the reduction in the percentage change in BFI is smaller than those in the CBF estimates.

4. Discussions and Conclusions

The use of NIRS and ICG in assessing cerebral haemodynamic variables has been attempted by many research groups. It has been reported that the qualitative shape of the measured tissue ICG concentration time curves can reflect the health of cerebral

perfusion.^{36,37} However, turning the tissue ICG time-concentration curves into quantitative CBF estimates, in ml/100g/min, or BFIs is more difficult and controversial. In this paper, we show through computer simulations that CBFs (absolute and relative) and BFIs (relative) estimated using the MBLL method (one detector) are heavily weighted towards the extracerebral blood flow.

The PPL method (two detectors) improves the sensitivities of the CBF estimates (absolute and relative) and BFIs (relative) to the underlying real CBF changes and reduces the influence of varying extracerebral blood flows (increasing robustness). Accurate quantification of absolute CBFs in ml/100g/min using this method, on the other hand, is difficult because the PPL method involves the estimation of partial pathlengths using computer simulations and therefore requires very accurate measurements of optical properties in each layer which are difficult to obtain in practice. As for BFI as a relative measure, it should be noted that the initial rise of a tissue ICG concentration time curve is not linear and subsequently the corresponding BFI does not increase linearly with the underlying real CBF. This explains the lack of linearity of BFIs we found in Figures 3(e), 3(f), 4(e), 4(f), 5(e) and 5(f). Our results suggest that using CBF estimates obtained from the PPL method as relative measures to quantify percentage changes from a baseline value is by far the most reliable approach to assess cerebral perfusion. Different extracerebral thicknesses also do not seem to influence these percentage changes significantly as demonstrated in Figure 3(d) and 4(d).

The problem becomes more complicated when the dispersion in the vasculature is taken into account. Figure 5 shows that CBF estimates and BFIs are biased in the presence of dispersion using even the PPL method. This is in fact a more fundamental problem of the dilution indicator methodology. The IRF approach cannot distinguish tracer dispersion in the feeding vessels, i.e. $[ICG(t)]_{art}$ from tracer retention in the capillary bed of the field of view, i.e. $[ICG(t)]_{int}$.^{20,38} This limitation is particularly relevant in NIRS measurements because $[ICG(t)]_{art}$ is often measured at a peripheral site (e.g. nose or ear lobe) which is some distance away from the actual feeding vessels in the brain. It has been suggested that resolving this problem requires the modelling of the vasculature which has been attempted in the MRI bolus tracking technique.³⁸

Apart from the PPL approach, one other possible method to estimate the optical properties in the two layers separately is to use the two layered optical model for inversion¹⁵. This has not been done here because it is generally not valid to use the same model for forward modelling and inversion. However, in general the two-layer model can be used for inversion in experimental measurements although there may be issues concerning long computation time and robustness.

We do not expect the two layered optical model used here to be able to accurately predict the actual optical data measured in a real human head. The two layered model is a gross simplification in that the complicated layered structure of a head is simplified to two flat layers corresponding to the extracerebral and intracerebral layers. Also, the cerebrospinal fluid has been ignored. Okada and Delpy²⁵ showed that the presence of low

scattering cerebrospinal fluid increases the partial pathlength in the brain and hence the actual optical measurements on the surface of the head may have a higher sensitivity to the real CBF than our results shown. In any case, the relatively effective method we found here, namely, the PPL method involves the weighted subtraction of μ_a as measured by two detectors. Any discrepancies due to the use of an inaccurate optical model apply equally to both μ_a and are substantially cancelled out in the subtraction. We therefore expect the results obtained from the PPL method using the proposed modelling technique to be sufficiently valid. In a recent experimental study in which the CBFs of 10 adult volunteers were increased (as assessed by transcranial Doppler) by the administration of acetazolamide, we found that the velocity of the middle cerebral artery as measured by transcranial Doppler was increased by $49 \pm 21\%$. However, the BFIs calculated using the MBLL method were unable to detect a statistically significant increase of the underlying CBF.⁹ We are currently investigating the use of the PPL method in this set of data.

When different baseline physiological or optical parameters (e.g. water content or μ_a^{bk}) are used, the absolute CBFs and BFIs obtained will also be different because the general distribution of light would have been changed as a result. We carried out a test (results not shown here) in which the extracerebral and intracerebral μ_a^{bk} were reduced to half of the values shown in Table 1. Unsurprisingly, we found different values for the absolute CBFs and BFIs. However, the central messages stated here still applied, i.e. (1) using the MBLL method, the absolute CBFs were significantly underestimated, (2) the PPL method improved the accuracy and robustness, (3) CBF estimates were best used as relative measures, and (4) dispersion of the AIF affected the CBF estimates.

Acknowledgements

The authors would like to thank Hamamatsu Photonics KK., UCL/UCH Trustees, EPSRC/MRC, Association of Anaesthetists of Great Britain and Ireland and Wellcome Trust (Grant No 075608) for their support in this work, and Dr Alwin Kienle for his help in the implementation of the 2 layer analytical model.

References

1. T. Durduran, G. Yu, M. G. Burnett, J. A. Detre, J. H. Greenberg, J. Wang, C. Zhou, A. G. Yodh, "Diffuse optical measurement of blood flow, blood oxygenation and metabolism in a human brain during sensorimotor cortex activation," *Opt. Lett.* **29**(15), 1766-1768 (2004).
2. C. E. Elwell, M. Cope, A. D. Edwards, J. S. Wyatt, D. T. Delpy, E. O. R. Reynolds, "Quantification of adult cerebral hemodynamics by near-infrared spectroscopy," *J. Appl. Physiol.* **77**(6), 2753-2760 (1994).
3. J. Patel, K. Marks, I. Roberts, D. Azzopardi, A. D. Edwards, "Measurement of cerebral blood flow in newborn infants using near infrared spectroscopy with indocyanine green," *Pediatr. Res.* **43**, 34-39 (1998).
4. R. Springett, Y. Sakata, D.T. Delpy, "Precise measurement of cerebral blood flow in newborn piglets from the bolus passage of indocyanine green," *Phys. Med. Biol.* **46**, 2209-2225 (2001).

5. C. R. J. C. Newton, D. A. Wilson, E. Gunnoe, B. Wagner, M. Cope, R. J. Traystman, "Measurement of Cerebral Blood Flow in Dogs with Near Infrared Spectroscopy in the Reflectance Mode Is Invalid," *J. Cereb. Blood Flow Metabol.* **17**, 695–703 (1997).
6. W. M. Kuebler, A. Sckell, O. Habler, M. Kleen, G. E. H. Kuhnle, M. Welte, K. Messmer, A. E. Goetz, "Noninvasive measurement of regional cerebral blood flow by near infrared spectroscopy and indocyanine green," *J. Cereb. Blood Flow Metabol.* **18**, 445-456 (1998).
7. F. Gora, S. Shinde, C. E. Elwell, J. C. Goldstone, M. Cope, D. T. Delpy, M. Smith, "Measurement of cerebral blood flow in adults using near infrared spectroscopy and indocyanine green," *J. Neurosurgical Anesthesiology* **14**, 218-222 (2002).
8. B. P. Wagner, S. Gertsch, R. A. Ammann, J. Pfenninger, "Reproducibility of the blood flow index as noninvasive, bedside estimation of cerebral blood flow," *Intensive Care Medicine* **29**, 196-200 (2003).
9. I. Tachtsidis, T. S. Leung, M. Tisdall, D. T. Delpy, M. Smith, C. E. Elwell, 2006 "Cerebral blood flow assessment with indocyanine green bolus transit detection by near-infrared spectroscopy before and after acetazolamide provocation in humans," in *Biomedical Optics 2006 Technical Digest* (Optical Society of America, Washington, DC, 2006), ME67.
10. K. Zierler, "Equations for measuring blood flow by external monitoring of radioisotopes," *Circ. Res.* **16**, 309-321 (1965).

11. G. T. Gobbel, J. R. Fike, "A deconvolution method for evaluating indicator-dilution curves," *Phys. Med. Biol.* **39**, 1833-1854 (1994).
12. D. W. Brown, P. Picot, J. Gharavi, R. Springett, D.T. Delpy, R. Menon, V. Han, T. Y. Lee, "Quantitative NIRS measurement of cerebral hemodynamics in newborn piglets," *Pediatr. Res.* **51**, 564-570 (2002).
13. E. Keller, A. Nadler, H. Alkadhi, S. S. Kollias, Y. Yonekawa, P. Niederer, "Noninvasive measurement of regional cerebral blood flow and regional cerebral blood volume by near-infrared spectroscopy and indocyanine green dye dilution," *NeuroImage* **20**, 828-839 (2003).
14. R. D. Rothoerl, K. M. Schebesch, R. Faltermeier, C. Woertgen, A. Brawanski, "Lack of correlation between Xenon¹³³ and near infrared spectroscopy/indocyanine green rCBF measurements," *Neurological Research* **25(5)**, 528-532 (2003).
15. A. Kienle, M. S. Patterson, N. Dognitz, R. Bays, G. Wagnieres, H. van den Bergh, "Noninvasive determination of the optical properties of two-layered turbid media," *Appl. Opt.* **37(4)**, 779-791 (1998).
16. P. Meier, K. L. Zierler, "On the theory of the indicator-dilution method for measurement of blood flow and volume," *J. Appl. Physiol.* **6(12)**, 731-743 (1954).
17. L. Friberg, J. Kastrup, M. Hansen, J. Bulow, "Cerebral effects of scalp cooling and extracerebral contribution to calculated blood flow values using the intravenous ¹³³Xe technique," *Scand. J. Clin. Lab. Invest.* **46**, 375-379 (1986).
18. R. M. P. Doornbos, R. Lang, M. C. Aalders, F. W. Cross, H. J. C. M. Sterenberg, "The determination of *in vivo* human tissue optical properties and absolute

- chromophore concentrations using spatially resolved steady-state diffuse reflectance spectroscopy,” *Phys. Med. Biol.* **44**, 967-981 (1999).
19. J. S. Wyatt, M. Cope, D. T. Delpy, C. E. Richardson, A. D. Edwards, S. Wray, E. O. Reynolds, “Quantitation of cerebral blood volume in human infants by near-infrared spectroscopy,” *J. Appl. Physiol.* **68**, 1086-1091 (1990).
 20. F. Calamante, D. G. Gadian, A. Connelly, “Delay and dispersion effects in dynamic susceptibility contrast MRI: simulations using singular value decomposition,” *Magn. Reson. Med.* **22**, 466-473 (2000).
 21. R. W. Stow, P. S. Hetzel, “An empirical formula for indicator-dilution curves as obtained in human beings,” *J. Appl. Physiol.*, **7**, 161-167 (1954).
 22. K. Murase, M. Shinohara, Y. Yamazaki, “Accuracy of deconvolution analysis based on singular value decomposition for quantification of cerebral blood flow using dynamic susceptibility contrast-enhanced magnetic resonance imaging,” *Phys. Med. Biol.* **46**, 3146-3159 (2001).
 23. M. Kohl-Bareis, H. Obrig, J. Steinbrink, J. Malak, K. Uludag, A. Villringer, “Noninvasive monitoring of cerebral blood flow by a dye bolus method: separation of brain from skin and skull signals,” *J. Biomed. Opt.* **7(3)**, 464-470 (2002).
 24. P. Mansfield, “Imaging by Nuclear Magnetic Resonance,” *J. Phys. E: Sci. Instrum.* **21**, 18-30 (1988).
 25. E. Okada, D. T. Delpy, “Near-infrared light propagation in an adult head model. I. Modelling of low-level scattering in the cerebrospinal fluid layer,” *Appl. Opt.* **42**, 2906-2914 (2003).

26. M. Essenpreis, C. E. Elwell, P. van der Zee, S. R. Arridge, D. T. Delpy, "Spectral dependence of temporal point spread functions in human tissues," *Appl. Opt.* **32**, 418-425 (1993).
27. D.M. Hueber, M.A. Franceschini, H.Y. Ma, Q. Zhang, J.R. Ballesteros, S. Fantini, D. Wallace, V. Ntziachristos, B. Chance, "Non-invasive and quantitative near-infrared haemoglobin spectrometry in the piglet brain during hypoxic stress, using a frequency-domain multidistance instrument," *Phys. Med. Biol.* **46**, 41-62 (2001).
28. Y. Hoshi, M. Shimada, C. Sato, Y. Iguchi, "Reevaluation of near-infrared light propagation in the adult human head: implications for functional near-infrared spectroscopy," *J. Biomed. Opt.* **10(6)**, 064032 (2005).
29. S.J. Matcher, C.E. Cooper, "Absolute quantification of deoxyhaemoglobin concentration in tissue near infrared spectroscopy," *Phys. Med. Biol.* **39**, 1295-1312 (1994)
30. P. van der Zee, M. Essenpreis, D. T. Delpy, "Optical properties of brain," *Proc SPIE* **1888**, 454-465 (1993).
31. S. J. Matcher, M. Cope, D. T. Delpy, "In vivo measurements of the wavelength dependence of tissue-scattering coefficients between 760 and 900 nm measured with time-resolved spectroscopy," *Appl. Opt.* **36**, 386-396 (1997).
32. A. Duncan, J. H. Meek, M. Clemence, C. E. Elwell, P. Fallon, L. Tyszczuk, M. Cope, D. T. Delpy, "Measurement of cranial optical-path length as a function of age using phase-resolved near-infrared spectroscopy," *Pediatr. Res.* **39(5)**, 889-894 (1996).

33. M. Hiraoka, F. Firbank, M. Essenpreis, M. Cope, S. R. Arridge, P. van der Zee, D. T. Delpy, "A Monte Carlo investigation of optical pathlength in inhomogeneous tissue and its application to near-infrared spectroscopy," *Phys. Med. Biol.* **38**, 1859-1876 (1993).
34. W. H. Press, S. A. Teukolsky, W. T. Vetterling, B. P. Flannery, *Numerical recipes in C, 2nd Ed.* (Cambridge University Press, 1992).
35. L. Ostergaard, R. M. Weisskoff, D. A. Chesler, C. Gyldensted, B. R. Rosen, "High resolution measurement of cerebral blood flow using intravascular tracer bolus passages. Part I: Mathematical approach and statistical analysis," *Magn. Reson. Med.* **36**, 715-725 (1996).
36. E. Keller, M. Wolf, M. Martin, Y. Yonekawa, "Estimation of cerebral oxygenation and hemodynamics in cerebral vasospasm using indocyanine green dye dilution and near infrared spectroscopy," *J. Neurosurgical Anesthesiology* **13**(1), 43-48 (2001).
37. A. Liebert, H. Wabnitz, J. Steinbrink, M. Moller, R. Macdonald, H. Rinneberg, A. Villringer, H. Obrig, "Bed-side assessment of cerebral perfusion in stroke patients based on optical monitoring of a dye bolus by time-resolved diffuse reflectance," *NeuroImage* **24**, 426-435 (2005).
38. L. Ostergaard, D. A. Chesler, R. M. Weisskoff, A. G. Sorensen, B. R. Rosen, "Modeling cerebral blood flow and flow heterogeneity from magnetic resonance residue data," *J. Cereb. Blood Flow Metab.* **19**, 690-699 (1999).

Table 1 Physiological and optical parameters (baseline value): ⁺ denotes the parameter whose value is to be changed in the numerical experiments

	Extracerebral	Intracerebral (grey matter)
Blood volume (ml/100g)	0.7	4
Total Hb concentration, [HbT] (μM)	11	61
Blood flow (ml/100g/min)	6.5 ⁺	60 ⁺
Mean transit time (s)	6.5	4.0
Water content (%)	70	71
Background absorption coefficient, μ_a^{bk} (mm^{-1})	0.015	0.023
Dispersion, β (s)	6	0 ⁺

Table 2 Parameters used in the three numerical experiments

Numerical experiments	Extracerebral blood flow (ml/100g/min)	Cerebral blood flow (ml/100g/min)	Dispersion factor in the intracerebral layer, β (s)
1	6.5	48, 54, 60, 66, 72	0
2	5.2, 5.85, 6.5, 7.15, 7.8	60	0
3	6.5	60	0, 0.25, 0.5, 0.75, 1

List of figure captions

Figure 1 (a) Modelled and experimentally measured arterial input function $[ICG(t)]_{art}$, (b) Modelled tissue ICG concentration time curves in the extracerebral layer $[ICG(t)]_{ext}$ and intracerebral layer $[ICG(t)]_{int}$

Figure 2 (a) Tissue ICG time-concentration curves calculated by the MBLL method using detector 2 (SD spacing = 50 mm), $[ICG(t)]_{det2}$ with three different dispersion factors, $\beta = 0, 0.5$ and 1 s; (b) Tissue ICG time-concentration curves calculated by the PPL method using detectors 1 and 2 (SD spacings = 45 and 50 mm), $[ICG(t)]_{det1\&2}$ with three different dispersion factors, $\beta = 0, 0.5$ and 1 s.

Figure 3 Numerical experiment 1: the extracerebral blood flow (the upper layer) was kept constant at 6.5 ml/100g/min and the real CBF (the lower layer) varied between -20% and 20% of its baseline value at 60 ml/100g/min. The three panels on the left (a,c and e) are results obtained using the MBLL method while the other three on the right (b, d and f) obtained using the PPL method. Results are presented as absolute values (ml/100g/min) for estimated CBFs in panels (a) and (b), and as relative values (% change from the middle value) for estimated CBFs and BFIs in panels (c), (d), (e) and (f). Different thicknesses of the extracerebral layer at 8 (\diamond), 10 (+) and 12 (\circ) mm were used. The dotted line represents the ideal estimation of CBF which follows exactly the real CBF.

Figure 4 Numerical experiment 2: the CBF (the lower layer) was kept constant at 60 ml/100g/min and the extracerebral blood flow (the upper layer) varied between -20% and 20% of its nominal value at 6.5 ml/100g/min. The three panels on the left (a,c and e) are results obtained using the MBLL method while the other three on the right (b, d and f) obtained using the PPL method. Results are presented as absolute values (ml/100g/min) for estimated CBFs in panels (a) and (b), and as relative values (% change from the middle value) for estimated CBFs and BFIs in panels (c), (d), (e) and (f). Different thicknesses of the extracerebral layer at 8 (\diamond), 10 (+) and 12 (\circ) mm were used. The dotted line represents the ideal estimation of CBF which is not biased by the extracerebral blood flow.

Figure 5 Numerical experiment 3: both the CBF (the lower layer) and the extracerebral blood flows (the upper layer) were kept constant at 60 and 6.5 ml/100g/min respectively. The dispersion factor in the intracerebral layer, β was varied between 0 and 1 s (step size of 0.25). The three panels on the left (a,c and e) are results obtained using the MBLL method while the other three on the right (b, d and f) obtained using the PPL method. Results are presented as absolute values (ml/100g/min) for estimated CBFs in panels (a) and (b), and as relative values (% change from the first value when $\beta = 0$ s) for estimated CBFs and BFIs in panels (c), (d), (e) and (f). Results were calculated with thicknesses of the extracerebral layer at 8 (\diamond), 10 (+) and 12 (\circ) mm. The dotted line represents the ideal estimation of CBF which is not biased by any dispersion in the vasculature.

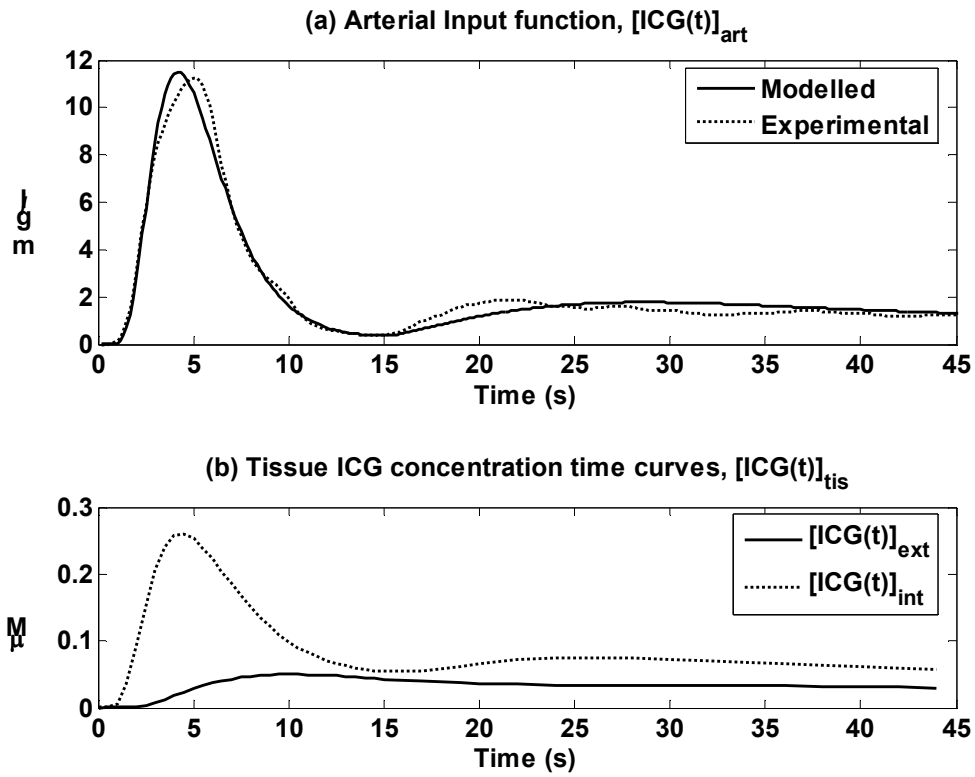


Figure 1 (a) Modelled and experimentally measured arterial input function $[ICG(t)]_{art}$, (b) Modelled tissue ICG concentration time curves in the extracerebral layer $[ICG(t)]_{ext}$ and intracerebral layer $[ICG(t)]_{int}$

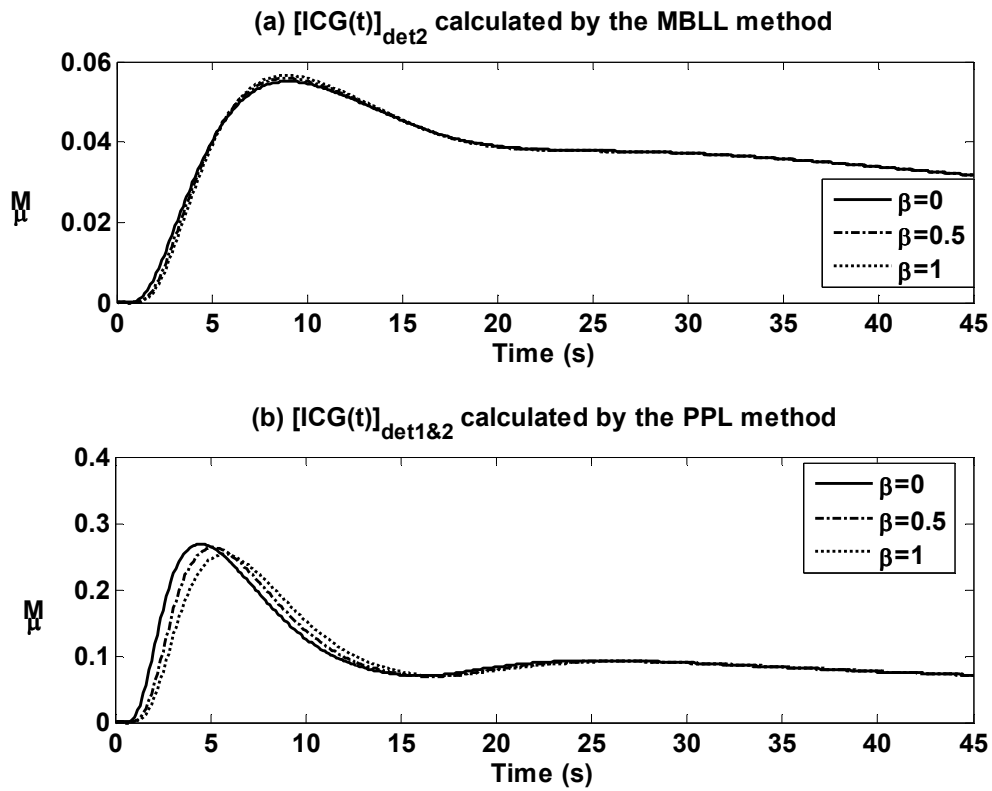


Figure 2 (a) Tissue ICG time-concentration curves calculated by the MBLL method using detector 2 (SD spacing = 50 mm), $[ICG(t)]_{det2}$ with three different dispersion factors, $\beta = 0, 0.5$ and 1; (b) Tissue ICG time-concentration curves calculated by the PPL method using detectors 1 and 2 (SD spacings = 45 and 50 mm), $[ICG(t)]_{det1\&2}$ with three different dispersion factors, $\beta = 0, 0.5$ and 1

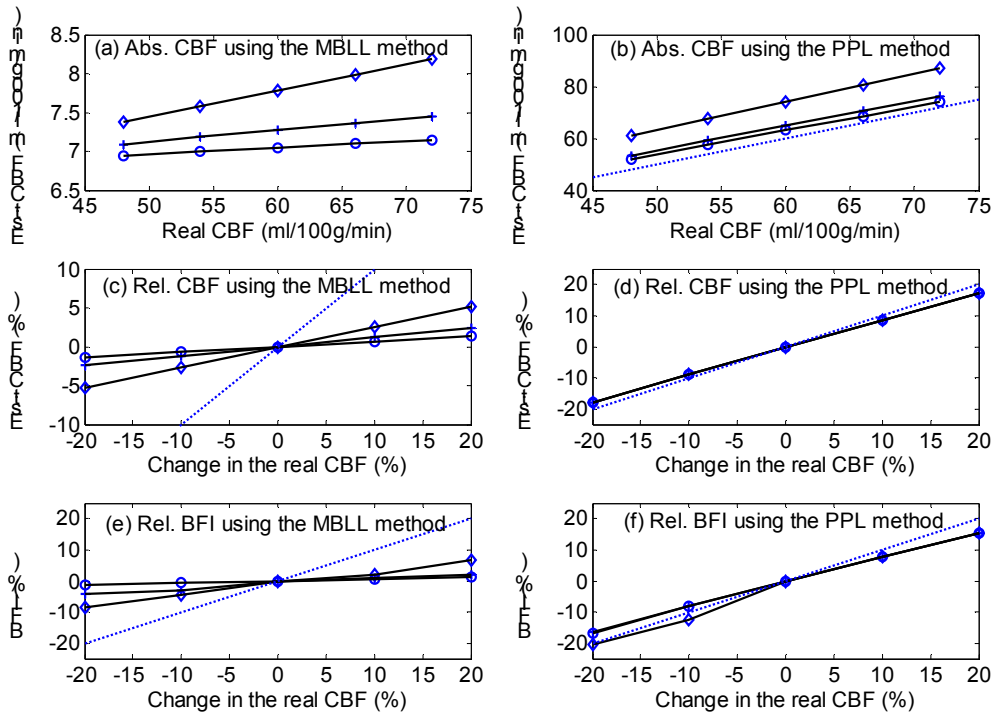


Figure 3 Numerical experiment 1: the extracerebral blood flow (the upper layer) was kept constant at 6.5 ml/100g/min and the real CBF (the lower layer) varied between -20% and 20% of its baseline value at 60 ml/100g/min. The three panels on the left (a,c and e) are results obtained using the MBLL method while the other three on the right (b, d and f) obtained using the PPL method. Results are presented as absolute values (ml/100g/min) for estimated CBFs in panels (a) and (b), and as relative values (% change from the middle value) for estimated CBFs and BFIs in panels (c), (d), (e) and (f). Different thicknesses of the extracerebral layer at 8 (\diamond), 10 (+) and 12 (\circ) mm were used. The dotted line represents the ideal estimation of CBF which follows exactly the real CBF.

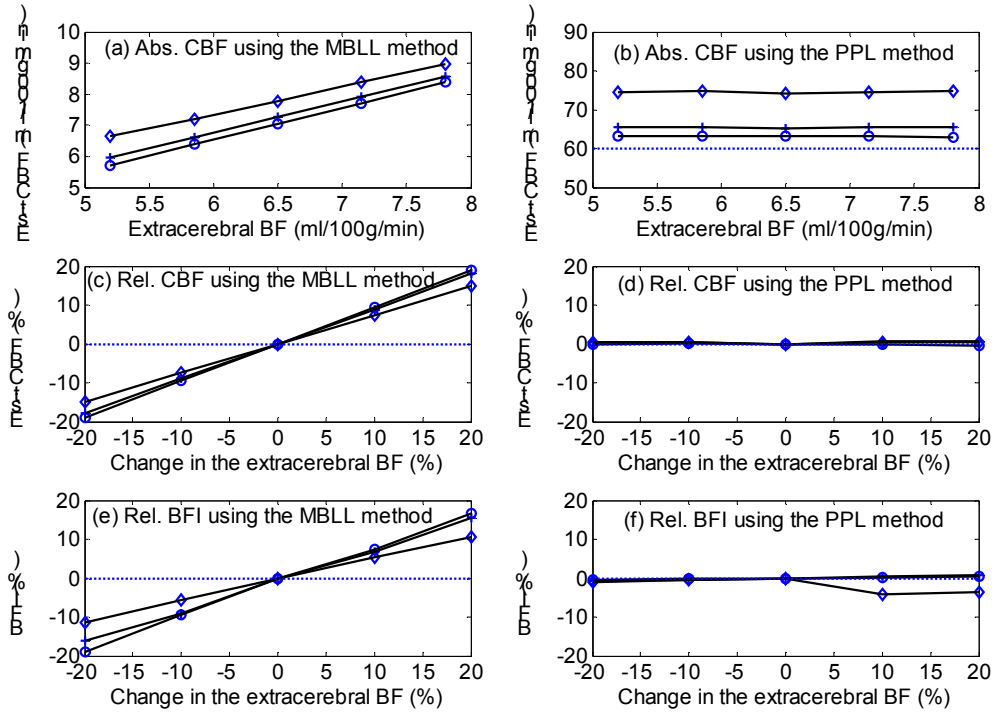


Figure 4 Numerical experiment 2: the CBF (the lower layer) was kept constant at 60 ml/100g/min and the extracerebral blood flow (the upper layer) varied between -20% and 20% of its nominal value at 6.5 ml/100g/min. The three panels on the left (a,c and e) are results obtained using the MBLL method while the other three on the right (b, d and f) obtained using the PPL method. Results are presented as absolute values (ml/100g/min) for estimated CBFs in panels (a) and (b), and as relative values (% change from the middle value) for estimated CBFs and BFIs in panels (c), (d), (e) and (f). Different thicknesses of the extracerebral layer at 8 (\diamond), 10 (+) and 12 (\circ) mm were used. The dotted line represents the ideal estimation of CBF which is not biased by the extracerebral blood flow.

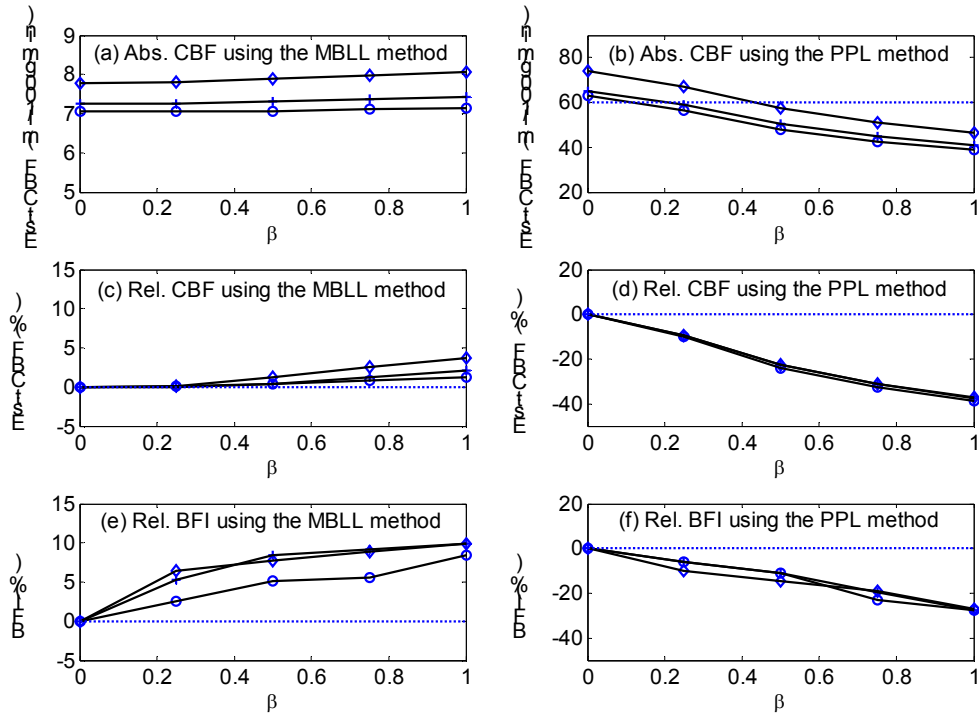


Figure 5 Numerical experiment 3: both the CBF (the lower layer) and the extracerebral blood flows (the upper layer) were kept constant at 60 and 6.5 ml/100g/min respectively. The dispersion factor in the intracerebral layer, β was varied between 0 and 1 (step size of 0.25). The three panels on the left (a,c and e) are results obtained using the MBLL method while the other three on the right (b, d and f) obtained using the PPL method. Results are presented as absolute values (ml/100g/min) for estimated CBFs in panels (a) and (b), and as relative values (% change from the first value when $\beta = 0$) for estimated CBFs and BFIs in panels (c), (d), (e) and (f). Results were calculated with thicknesses of the extracerebral layer at 8 (\diamond), 10 (+) and 12 (\circ) mm. The dotted line represents the ideal estimation of CBF which is not biased by any dispersion in the vasculature.